

Simulation Study of the Robust Closed-Loop Control of a 2D High-Lift Configuration

B. Günther, A. Carnarius and F. Thiele

*Institute of Fluid Mechanics and Engineering Acoustics, Berlin University of Technology,
Müller-Breslau-Str. 8, 10623 Berlin, Germany,
Bert.Guenther@cfm.tu-berlin.de*

R. Becker and R. King

*Department of Process and Plant Technology, Berlin University of Technology,
Hardenbergstr. 36a, 10623 Berlin, Germany,
Ralf.Becker@tu-berlin.de*

Abstract. The investigation focuses on the closed-loop separation control of a two dimensional high-lift configuration in a numerical simulation study. The lift is to be controlled by adjusting the non-dimensional intensity of the harmonic excitation near the leading edge of the single slotted flap. Since control laws based on a high-dimensional discretisation or low-dimensional description of the Navier–Stokes equations are not applicable in real-time, this investigation presents a fast and efficient controller synthesis methodology employing robust methods. This offers real-time capability for future experimental implementations. In spite of the nonlinear and infinite-dimensional Navier-Stokes equations, it is surprising to observe that the dynamic behaviour appears very simple. This input-output behaviour in the vicinity of set points can be empirically approximated by stable linear black-box models of second order. Based on these, a simple robust controller is synthesised that autonomously adjusts the excitation such that a desired lift is obtained.

Key words: high-lift, active flow control, RANS, incompressible flow, robust, closed-loop.

1. Introduction

The wings of commercial aircraft must generate a tremendous amount of lift during take-off and landing in order to reduce ground speeds and runway lengths. Instead of incorporating complex, heavy and expensive multi-element high lift devices, single flaps without slats are desirable. Such flaps can however only be applied if flow separation at high flap angles can be avoided. Experimental investigations [1] as well as numerical simulations [2] have shown that flap separation can be significantly delayed by periodic excitation near the flap leading edge in the case of low and high Reynolds numbers [3] and the lift can be enhanced.

In further investigations [4, 5] oscillatory suction and blowing was found to be much more efficient than steady blowing with respect to lift. The process becomes very efficient if the excitation frequencies correspond to the most unstable frequencies of the free shear layer, generating arrays of spanwise vortices that are convected downstream and continue to mix across the shear layer. In order to create an effective and efficient control method, previous studies have primarily focused on the

parameters of the excitation apparatus itself. Overviews are given by Wygnanski and Gad-el-Hak [6, 7].

The present investigation focuses on lift control of a two dimensional, three element high-lift configuration in a numerical simulation study. The lift is to be controlled by adjusting the amplitude of the harmonic excitation near the leading edge of the single slotted flap. Open-loop control, however, suffers from two severe drawbacks related to uncertainty. First, it has to be based on a profound knowledge of the flow system considered in order to correctly invert the input-output relation from the actuator to the quantity being controlled. If this relation is not fully known, open-loop performance will deteriorate if not fail. A second source of uncertainty will always be given by disturbances, especially when leaving the well-defined conditions of a laboratory wind tunnel. To overcome these problems, closed-loop control is employed here to control the high-lift configurations.

Keeping the requirement of a real time capability in mind, thus excluding feedback control based on a numerical solution of the Navier–Stokes equations, only three approaches seem to be promising:

- 1) The best results will be obtained by nonlinear controllers exploiting low-dimensional models that describe the nonlinear physics, i.e. Galerkin or vortex models. However, these models are presently restricted to rather simple flow configurations and will still rely on a rather detailed knowledge of the system.
- 2) In adaptive control [8], models are identified online. This information is then used to adapt the controller in real time. As an alternative, model-free methods [9] can also be applied in adaptive control, such as extremum seeking control.
- 3) A fast and cost-effective controller synthesis employing robust methods is possible as a third alternative based on a family of linear or nonlinear black-box models [8, 10] identified offline. This latter approach will be used here.

The paper is organised as follows: A description of the configuration is given in section 2. Section 3 describes controller design and simulation results. Finally, the results are summarized.

2. Flow configuration

2.1. GENERAL DESCRIPTION

The numerical test model represents the practically-relevant *SCCH* (**S**wept **C**onstant **C**hord **H**alf-model) high-lift configuration, which has already been used for several experimental studies targeting passive/active flow and noise control concepts [11, 12, 13]. In the experiments, the three-dimensional wing has a sweep angle of $\Phi = 30^\circ$ and a constant chord length in the spanwise direction. The numerical investigation is mainly focused on a 2D wing profile in order to reduce the computational costs.

The typical three-component setup consists of the main airfoil equipped with an extended slat of $0.158c$ relative chord length and an extended flap which has a relative chord length of $c_k = 0.254c$ (Fig. 1). All profiles have blunt trailing edges. The flap is situated at a fixed position underneath the trailing edge, forming a gap of $0.0202c$ and an overlap of $0.0075c$. The flap deflection angle was increased from the base value (32°) to a angle of 37° in order to maximise the recirculation above

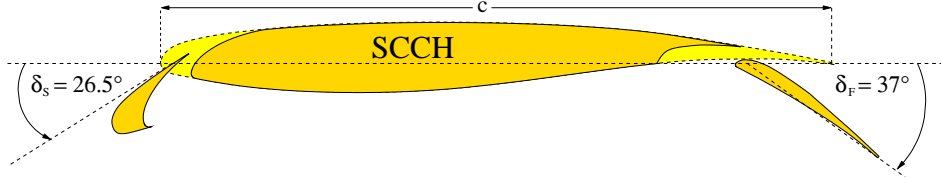


Figure 1: Sketch of the SCCH high-lift-configuration.

the flap. The angle of attack is fixed at 6° for the whole configuration. In addition, the flow over the flap is detached whereas the flow over the slat and the main wing are still fully attached.

In all numerical investigations the freestream velocity corresponds to a Reynolds number of $Re_c = 10^6$ based on the chord of the clean configuration (with retracted high-lift devices). This high Reynolds number is chosen to demonstrate the relevance to industrial applications.

2.2. NUMERICAL METHOD

All computational investigations have been carried out using the numerical code *ELAN* was developed at the Institute of Fluid Mechanics and Engineering Acoustics of the TU Berlin. The numerical method is based on a three-dimensional incompressible finite-volume scheme for solution of the Reynolds-averaged Navier–Stokes equations [14]. All URANS simulations are based on the statistical turbulence model LLR $k-\omega$ by Rung [15], which represents an improved two-equation eddy viscosity model formulated with special respect to the realisability conditions.

The computational c-type mesh consists of 90,000 cells in total with 15 chords upstream, above and below the configuration and 25 chords downstream. The non-dimensional wall distance of the first cell centre remains below $Y^+ = 1$ over the entire surface.

A separate study of the influence of time step size indicated that a typical time step of $\Delta t = 2.1 \times 10^{-3} c/u_\infty$ is sufficient to resolve the important flow structures. All computations presented here are based on $\Delta t = 1.26 \times 10^{-3} c/u_\infty$, which allows a resolution of 630 time steps per period of vortex-shedding in the unexcited case and 336 time steps per oscillation cycle for a non-dimensional oscillating frequency of $F^+ = 0.6$.

To model the excitation apparatus, a periodic suction/blowing type boundary condition is used. The perturbation to the flow field is introduced through the inlet velocity on a small wall section representing the excitation slot:

$$u_{exc}(t) = u_a \cdot \sin \left[\left(2\pi \frac{u_\infty}{c_k} F^+ \right) \cdot t \right] \quad \text{with} \quad u_a = u_\infty \sqrt{\frac{c}{H} C_\mu} \\ F^+ = f_{per} \cdot \frac{c_k}{u_\infty} \quad (1)$$

where F^+ is the non-dimensional perturbation frequency, C_μ is the non-dimensional steady momentum blowing coefficient, H is the slot width ($H = 0.001238 c_k$) and u_a is the amplitude velocity of the perturbation oscillation. The oscillating jet is emitted perpendicular to the wall segment of the excitation slot, and is located at 4.1% chord behind the flap leading edge.

2.3. UNEXCITED FLOW

As a first step, two-dimensional, unsteady investigations without excitation have been carried out. The flow field of the *SCCH*-configuration without excitation is characterised by massive separation above the upper surface of the flap. The mean separation point is located at 4.1% chord behind the flap leading edge, and downstream a large recirculation region occurs. The unsteady behaviour of separated flow is mainly governed by large vortices shed from the flap trailing edge that interact with the vortices generated in the shear-layer between the recirculation region and the flow passing through the slot between main airfoil and flap nose (Fig. 2(a)). The spectrum of the lift coefficient in Fig. 2(b) shows a dominant amplitude for a Strouhal number of the unexcited flow formed with the flap chord of $St_u = f \frac{c_k}{u_\infty} = 0.32$, mainly produced by this vortex shedding. The base flow configuration involving massive separation over the flap described above is undesirable, and the goal is to improve this using active flow control.

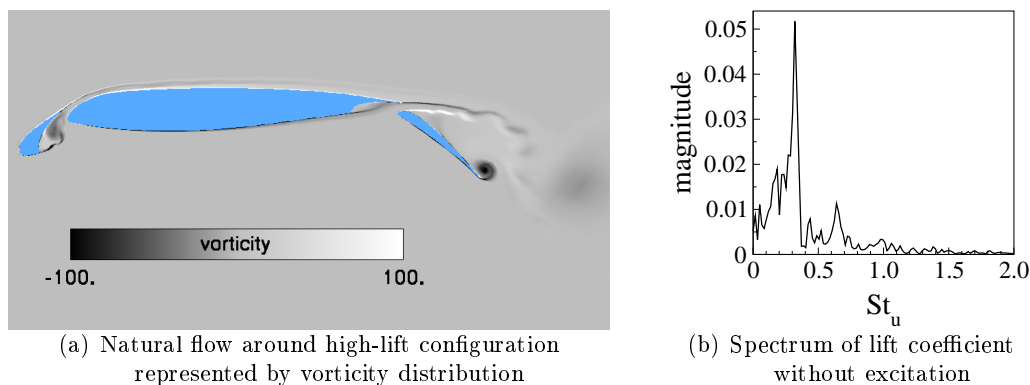


Figure 2: Numerical results of the unexcited flow

2.4. EXCITED FLOW

After the base flow investigations, flow control mechanisms are applied. All flow control computations use the baseline case solutions as initial flow conditions. In order to find an optimum excitation, simulations with different variable excitation parameters, such as excitation frequency, excitation intensity, blow out angle or duty cycle are performed (Fig. 3). The numerical investigations employed sinusoidal perturbation and periodic blowing in comparison to the experimental excitation mode [11]. The studies with variable excitation frequencies and intensities (Fig. 3(a) and 4(b)) show that active flow control by periodic blowing could not achieve the gain in lift seen for excitation by sinusoidal suction and blowing.

Periodic Excitation with different intensity

For the excited flow case periodic perturbations with an intensity of between $C_\mu = 10 \times 10^{-5}$ and $C_\mu = 500 \times 10^{-5}$ have been introduced. This excitation parameter has been selected as the control signal in order to design a robust controller. Compared to the detached, unexcited flow, the excited lift could be continuously increased with growing intensity. The maximum of lift can be identified for a harmonic excitation of

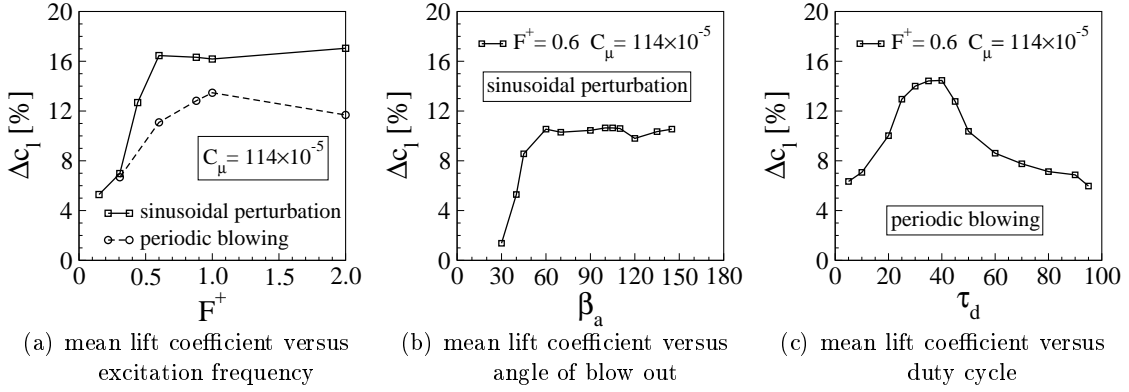


Figure 3: Numerical results of the excited flow

$C_\mu = 400 \times 10^{-5}$. In this case the lift coefficient can be enhanced by 19% compared to the baseline simulation (Fig. 4(b)).

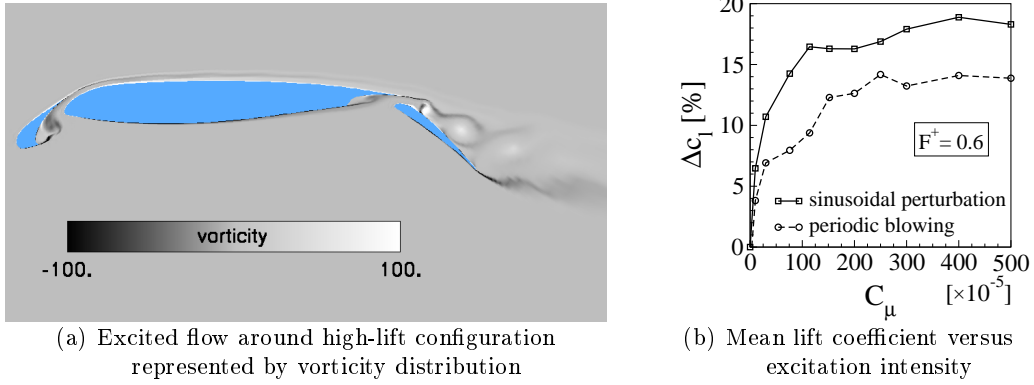


Figure 4: Numerical results of excitation with different intensities

The gain in lift by the excitation is mainly based on a change of flow direction at the trailing edge of the main airfoil. With the excited condition of flow above the flap the trailing edge departure angle is increased (compare Figs. 2(a) and 4(a)) and the pressure distribution above the main airfoil is enhanced. The natural flow above the flap is mainly governed by large-scale vortex shedding from the flap trailing edge, which is nearly eliminated in the optimal excited flow (see Fig. 2(a) and 4(a)). Small-sized vortices generated by periodic suction and blowing above the perturbation slit enable the transport of energy from the main flow to the recirculation near the wall. Thereby the time-average detachment position moves from less than 5% chord downstream to more than 12%, the recirculation area is reduced and the downflow condition is modified.

3. Robust control

Fig. 4(b) illustrates the benefits of periodic excitation (sinusoidal perturbation). The plot displays the time-averaged, steady-state input-output map of the configuration, i.e. the lift coefficient c_l versus excitation intensity C_μ . Excitation with low intensity

($C_\mu = 10$ to 100×10^{-5}) leads to a strong increase in lift (max. 17%). If C_μ becomes larger the lift shows a saturation behaviour.

The controller computes the non-dimensional intensity $C_\mu(\tau)$ of the harmonic excitation in order to track a desired lift coefficient $c_{l,desired}(\tau)$ referred to as the reference command in the following. Here, τ is the dimensionless time given in convective units. In control notation $C_\mu(\tau)$ is taken as the control signal and $c_l(\tau)$ as the system output to be controlled. Therefore, a classical closed-loop feedback control system as shown in Fig. 5 is used. The controller calculates the control signal $C_\mu(\tau)$ as function of the difference between $c_{l,desired}(\tau)$ and $c_l(\tau)$.

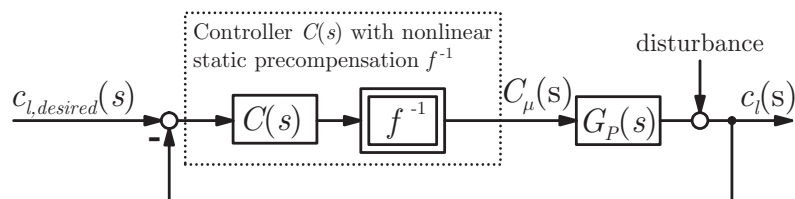


Figure 5: Control-loop with compensation of a variable static gain.

3.1. DYNAMIC SYSTEM BEHAVIOUR

In spite of the nonlinear and infinite dimensional Navier–Stokes equations, it is surprising that the dynamic behaviour of the lift $c_l(\tau)$ as a function of time looks very simple in step experiments (see Fig. 6). The plots on the left-hand and right-hand side display step responses for switching $C_\mu(\tau)$ on and off, respectively. All system responses can be approximated by stable linear black-box models $G_P(s)$ of first or second order [10].

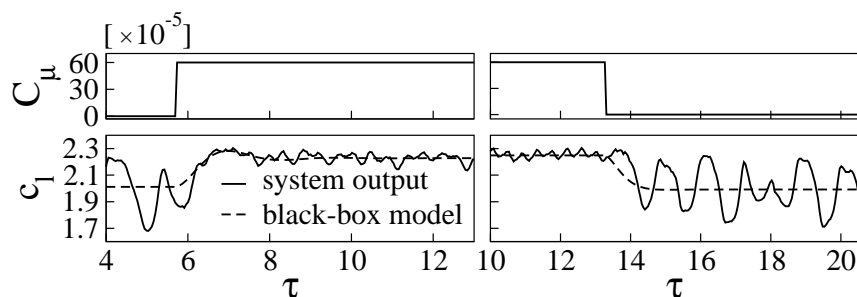


Figure 6: Identification of black-box models from step responses (left: switching $C_\mu(\tau)$ on; right: switching $C_\mu(\tau)$ off)

Due to the nonlinear characteristics of the investigated system, large ranges for the identified model parameters have to be accepted for various step heights and initial values of the control signal $C_\mu(\tau)$. To avoid a significant detuning of the controller $C(s)$, it is desirable to reduce the model uncertainty. As the steady-state gain $K_P = \lim_{s \rightarrow 0} G_P(s)$ of all identified models $G_P(s)$ shows a highly nonlinear dependence on the size of the control signal C_μ , i.e. the forcing amplitude, the inverse

f^{-1} of the steady-state input-output map $c_l = K_P(C_\mu) \cdot C_\mu = f(C_\mu)$ ($C_\mu = \text{const.}$, $\tau \rightarrow \infty$, see Fig. 4(b)) can be used to compensate for this nonlinearity as displayed in Fig. 5. Here, a simple exponential relation is fitted between the data points for sinusoidal perturbation in Fig. 4(b).

In order to describe the nonlinear behaviour of the real process, a family Π of linear black-box models $G_P(s) \in \Pi$ is identified from representative step experiments as illustrated in Fig. 6 for all relevant operating points. The black lines in Fig. 7 display the Bode magnitude (top) and phase (bottom) plots of the models $G_P(s) \in \Pi$. Due to the compensation f^{-1} , the steady-state gain of all models is about one. The spread of the cut-off frequencies is caused by the different dynamics of the experiments with the varying step heights for switching on (positive) and switching off (negative) cases. However, positive steps correspond to faster dynamics resulting in higher cut-off frequencies.

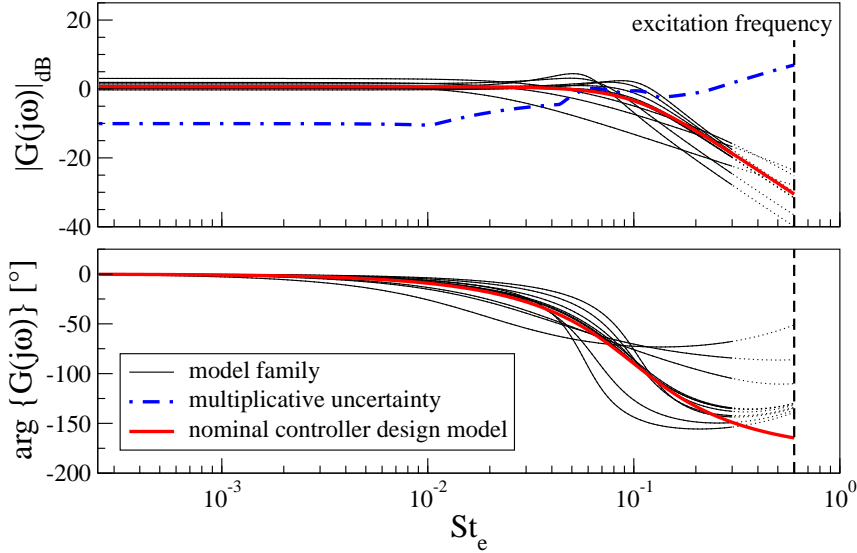


Figure 7: Frequency responses of the model family $G_P(s) \in \Pi$ with compensation of the nonlinear gain.

The flow system description by continuous black-box models is only valid for significantly lower frequencies than the excitation frequency, as illustrated in Fig. 7. Otherwise, the sinusoidal excitation signal will be distorted and the active flow excitation mechanism does not work properly. This upper bound for validity is illustrated by the dotted model frequency responses and the vertical dashed line for the excitation frequency.

3.2. DETERMINATION OF THE CONTROLLER DESIGN MODEL

A linear nominal model $G_n(s)$ with a multiplicative uncertainty description

$$l_M(\omega) = \max_{G_P \in \Pi} \left| \frac{G_P(j\omega) - G_n(j\omega)}{G_n(j\omega)} \right| \quad (2)$$

for the neglected or non-modelled dynamics is derived from the spreading model family $G_P(s) \in \Pi$, and these are then used for robust controller synthesis. Roughly

speaking, $l_M(\omega)$ gives the validity range of $G_n(j\omega)$. $G_n(s)$ and $l_M(\omega)$ are plotted in the Bode diagram in Fig. 7 with a thick solid and a dash-dotted line, respectively.

By searching for a nominal model $G_n(s)$ with the smallest uncertainty radius, it turns out that a simple second-order transfer function $G_n(s) = K/(1 + sT_1 + s^2T_2)$ can be used [10]. The parameters T_1 and T_2 are identified by solving an optimization problem such that the least mean square uncertainty radius is obtained.

3.3. CONTROLLER DESIGN

Due to the uncertainty of the identified models, robustly designed controllers are required to maintain closed-loop stability for all operating points. As a PI-controller $C_{PI}(s) = K(1 + 1/sT_I)$ is the most common controller for such systems, its application was tested first. Here, the PI-break frequency $\omega = 1/T_I$ was chosen near to the nominal model cut-off frequency as displayed in the Bode magnitude plot in Fig. 8. The thin solid line indicates the nominal model and the bold dash-dotted line indicates the PI-controller. In order not to amplify oscillations, only a moderate gain K was chosen for the first closed-loop studies in order to obtain high phase and gain margins. Additionally, as described below, the PI-structure was simplified to an I-structure $C_I(s) = 1/sT_I$ as illustrated in Fig. 8 by the bold solid line. Both controllers meet the robust stability requirement.

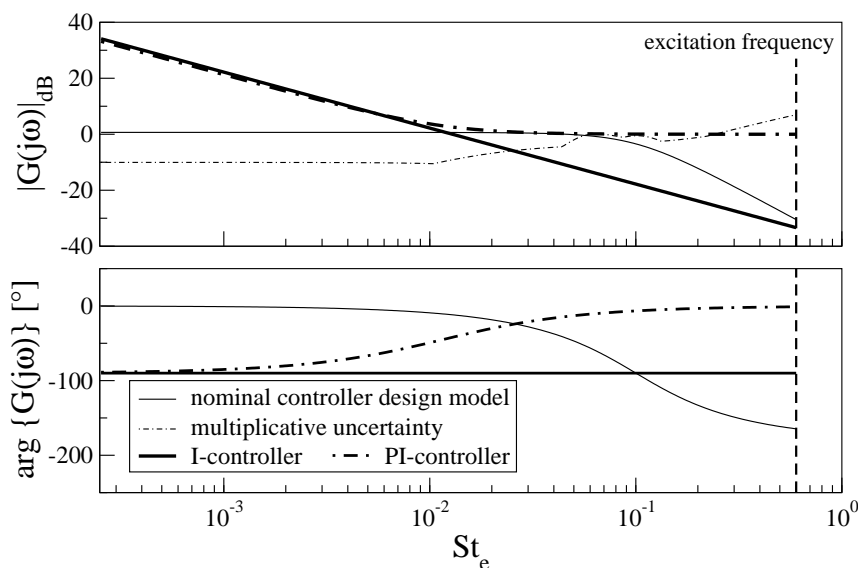


Figure 8: Frequency responses of the nominal controller design model $G_n(s)$, the corresponding multiplicative uncertainty $l_M(\omega)$, and the robust I- and PI-controllers $C_I(s)$ and $C_{PI}(s)$, respectively.

3.4. RESULTS FOR COMMAND TRACKING PERFORMANCE

In the left-hand time plot of Fig. 9, which shows the closed-loop command tracking performance of the PI-controller, it is seen that the controlled system output $c_l(\tau)$ follows the step input reference command $c_{l,desired}(\tau)$ although with strong oscillations. Despite a closed-loop design that does not amplify oscillations in the case of linear systems due to the high gain and phase margins, the flow system still shows

a strong nonlinear behaviour with oscillating dynamics leading to this poor closed-loop performance. Even the variation of the controller parameters toward smaller gains K and break frequencies $\omega = 1/T_I$ does not reject or damp the oscillations. Corresponding results are not shown here.

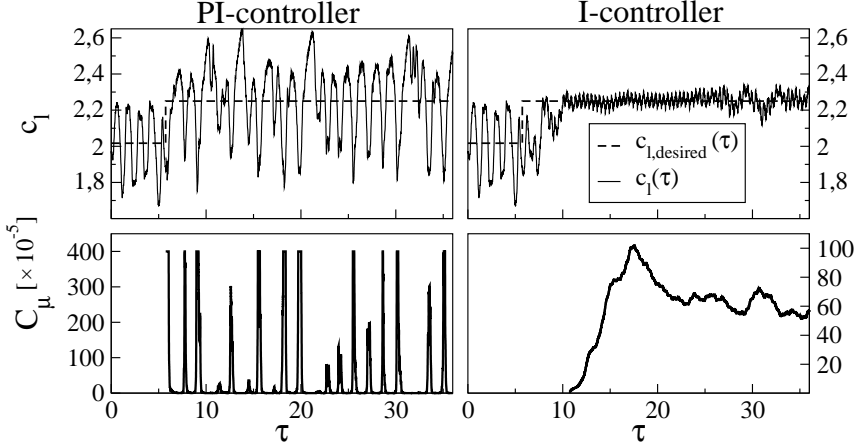


Figure 9: Comparison of the tracking responses of the robust PI- and I-controller. (- - reference command $c_{l,desired}(\tau)$, — controlled system output $c_l(\tau)$)

Since the robust PI-controller does not reject the oscillations, which are inherent to the flow system, a modified controller structure with low frequency response magnitude in the range of the oscillations is chosen next. The robust I-controller described above is the simplest and most obvious candidate for this purpose, see the tracking response in the right-hand time plot of Fig. 9. However, the controlled lift follows the reference command signal thereby damping the oscillations to low acceptable level.

In order to achieve faster closed-loop tracking responses, simulation studies with higher I-controller crossover frequencies $\omega = 1/T_I$ have been carried out. Again, non-acceptable oscillations occurred in these cases with smaller gain and phase margins. Again, corresponding results are not shown in this paper. Obviously, a sufficient low frequency response magnitude is needed to damp the inherent oscillations in the range of the excitation frequency and this is not given for higher I-controller crossover frequencies.

4. Conclusions

This paper describes a successful approach for closed-loop separation control by active means on a high-lift configuration, i.e. a two dimensional wing with a slat and a single slotted trailing edge flap. Well-known local periodic forcing near the leading edge of the flap is used to excite the flow in order to control flow separation and, hence, the corresponding lift. Since closed-loop flow control suffers from the lack of sufficiently simple, low-dimensional controller design models based on the Navier–Stokes equations, an empirical family of linear black-box models is identified from representative simulation studies, which are then used for robust controller design. Loop shaping yields a linear controller with I-structure and this offers real-time capability for future experimental implementations. However, the inherent

non-linear oscillating flow system behaviour imposes a limitation on the achievable performance, i.e. the closed-loop crossover frequency needs to be sufficiently smaller than the oscillations in the range of the excitation frequency.

Acknowledgements

The research project is funded by Deutsche Forschungsgemeinschaft (German Research Foundation) as part of the Collaborative Research Centre 557 *Complex turbulent shear flows* at TU Berlin.

References

- [1] F.H. Tinapp. *Aktive Kontrolle der Strömungsablösung an einer Hochauftriebs-Konfiguration*. PhD thesis, Technische Universität Berlin, 2001.
- [2] M. Schatz and F. Thiele. Numerical study of high-lift flow with separation control by periodic excitation. *AIAA Paper 2001-0296*, 2001.
- [3] M. Schatz, F. Thiele, R. Petz, and W. Nitsche. Separation control by periodic excitation and its application to a high lift configuration. *AIAA Paper 2004-2507*, 2004.
- [4] S.S. Ravindran. Active control of flow separation over an airfoil. TM-1999-209838, NASA, Langley, 1999.
- [5] J.F. Donovan, L.D. Kral, and A.W. Cary. Active flow control applied to an airfoil. *AIAA Paper 98-0210*, 1998.
- [6] I. Wygnanski. The variables affecting the control separation by periodic excitation. *AIAA Paper 2004-2505*, 2004.
- [7] M. Gad-el Hak. Flow control: The future. *Journal of Aircraft*, 38(3), 2001.
- [8] R. King, R. Becker, and M. Garwon. Robust and adaptive closed-loop control of separated shear flows. *AIAA-Paper 2004-2519*, 2004.
- [9] R. Becker, R. King, R. Petz, and W. Nitsche. Adaptive closed-loop separation control on a high-lift configuration using extremum seeking. *AIAA-Paper 2006-3493*, 2006.
- [10] R. Becker, M. Garwon, C. Gutknecht, G. Bärwolff, and R. King. Robust control of separated shear flows in simulation and experiment. *Journal of Process Control*, Vol. 15:pp. 691–700, 2005.
- [11] B. Günther, F. Thiele, R. Petz, W. Nitsche, J. Sahner, T. Weinkauff, and H.-C. Hege. Control of separation on the flap of a three-element high-lift configuration. *AIAA Paper 2007-265*, 2007.
- [12] M. Schatz, B. Günther, and F. Thiele. Computational investigation of separation control for high-lift airfoil flows. In R. King, editor, *‘Active Flow Control’, Notes on Numerical Fluid Mechanics and Multidisciplinary Design*, volume Vol. 95. Springer Verlag, 2007.
- [13] K. Kaepernick, L. Koop, and K. Ehrenfried. Investigation of the unsteady flow field inside a leading edge slat cove. In *11th AIAA/CEAS Aeroacoustics Conference (26th Aeroacoustics Conference)*, Monterey, CA, USA, 2005.
- [14] L. Xue. *Entwicklung eines effizienten parallelen Lösungsalgorithmus zur dreidimensionalen Simulation komplexer turbulenter Strömungen*. PhD thesis, Technische Universität Berlin, 1998.
- [15] T. Rung and F. Thiele. Computational modelling of complex boundary-layer flows. In *9th Int. Symp. on Transport Phenomena in Thermal-Fluid Engineering*, Singapore, 1996.